https://erjm.journals.ekb.eg
ISSN: 1110-1180

DOI: ---------

ERJ
Engineering Research Journal
Faculty of Engineering
Menoufia University

Comparative Study on Using Steel and Glass Fiber Reinforced Polymer Rebars as Reinforcement on Flexural Behavior of Concrete Beams

Ahmed F. Elkhouly*, Magdy A. Tayel, and Hossam G. Sallam

Department of Civil Engineering, Faculty of Engineering, Menoufia University, Cairo, Egypt.
**(Corresponding author: ahmed.elkholy@sh-eng.menofia.edu.eg)*

ABSTRACT
Due to problem of steel corrosion and high cost, the use of glass fiber reinforced polymers (GFRP) has become more convenient to be used widely nowadays. This study implicated experimental, numerical, and analytical comparison between GFRP and steel RC beams. Twelve beams were tested under four-point flexural load till failure, The beams had a clear span of 2000 mm and a cross sectional area width and height of 120 mm and 300 mm, respectively. The beams were categorized into two groups (A and B) from these twelve beams according to reinforcement type (steel or GFRP). Group A consists of four beams while group B includes eight beams. Two reinforcement types were used: high tensile steel (10 mm dia.) and GFRP rebars (8 mm and 10 mm dia.) with reinforcement ratios 0.5% and 1%. Numerical study using ABAQUS 6.14 was performed with the following parameters: concrete strength, diameter of the reinforcing GFRP bars, reinforcement ratio, and type of reinforcement. According to test results, utilizing GFRP bars in beams of 25 MPa concrete strength increased the failure load by an average of 18% and 7% while beams of 35 MPa concrete strength increased by an average of 22% and 11% for beams of 0.5% and 1.0% reinforcement ratio, respectively. The mid-span deflection was dramatically increased when utilizing GFRP bars as opposed to steel bars. A comparison between experimental, analytical, and numerical results was done and showed good consistency.

Keywords: *Reinforced concrete beams; Flexural; GFRP bars; Concrete grades; Reinforcement ratio.*

1. Introduction

The issue of ageing infrastructure, particularly in relation to reinforced cement concrete, is one of the largest concerns of these days. Corrosion of the reinforcing steel is the main factor contributing to the deterioration of reinforced concrete structures [1]. The reason of the corrosion problem is the concrete cover's lack of protection. [2]. Using noncorrosive glass fiber-reinforced polymer (GFRP) rebars to reinforce concrete is a realistic option. High tensile strength, light weight, non-magnetism, and high stiffness-to-weight and strength-to-weight ratios represent some of the additional benefits of GFRP reinforcement. Because of these benefits, GFRP rebars are an attractive option for concrete building reinforcement [3]–[5]. Because of these benefits, glass fiber reinforced polymer (GFRP) bars can prolong the life of reinforced concrete structures and reduce maintenance, repair, and replacement costs [6], [7]. Although GFRP is an effective option for reinforcing, the design challenges it faces are distinct from those associated with conventional steel reinforced concrete. One major challenge is to take into account a brittle failure mode in GFRP-reinforced parts. The comparatively low rigidity of GFRP reinforcing bars is one of their main drawbacks. Thus, the serviceability limit states (deflection and cracking) rather than the ultimate limit states are frequently used to guide the design of GFRP-reinforced concrete members. GFRP bars fail quickly because they do not yield like steel bars do. Because of this, a number of codes and standards mandate that beams reinforced with glass fiber reinforced polymer (GFRP) bars be designed to be over-reinforced, meaning that the failure mechanism should be concrete compression rather than bar failure. The purpose of this beam design concept was to give the beam more time to deflect and warn of the need for repair before GFRP bars fall catastrophically [8].

The behavior of beams made of either normal-strength concrete (NSC) or high-strength concrete (HSC) and reinforced with FRP bars under flexural loading has been the subject of numerous studies [1], [3], [6]–[32]. Previous studies have shown that the behavior of concrete beams reinforced with fiber-reinforced polymer rebars was bilinear. The behavior of the uncracked beams is shown by the first portion of the curve up to cracking. The behavior of the broken beams with decreased rigidity is depicted in the second section. The ultra-high strength concrete reinforced

with GFRP rebars exhibited the same behavior [29]. The GFRP beams' flexural capacity rose in tandem with an increase in reinforcement ratio. GFRP-reinforced concrete beams have a greater maximum load than steel-reinforced concrete beams [32]. The GFRP-reinforced concrete beams had bigger cracks than the steel-reinforced concrete beams. Other serviceability restrictions on stress in GFRP bars are governed by the 0.5 mm crack width limit [1]. Compared to the NSC beams, the HSC beams had greater post-cracking flexural rigidity. Moreover, by spreading more cracks throughout the beams, the increased concrete strength and reinforcing ratio decreased crack widths. In comparison to steel-reinforced concrete beams, the GFRP-steel reinforced concrete beams exhibited crack breadth and deflection that appeared more quickly [9]. Compared to the normal beam, the beam strengthened with GFRP bars had more cracks [13], [15]. GFRP reinforced concrete beams have a higher deflection and can support a lower weight than steel reinforced concrete beams.

With varying concrete strengths, types of reinforcement, reinforcement ratios, and bar sizes, this study examines the flexural behavior of concrete beams reinforced with glass fiber reinforced polymer rebars (GFRP). Using four-point bending over a 2000 mm clear span, a total of 12 beams were tested till failure. The test findings are shown in terms of deflection, failure mode, initial cracking load, and failure load.

2. Experimental Investigation

Twelve beams were used in the test program divided into two groups (A and B) according to reinforcement type (steel or GFRP) and each group have two series of beams based on concrete grade. Group A consists of four beams while group B includes eight beams. Series I and III (six beams) were cast with concrete having a characteristic strength of 25 MPa while series II and IV (six beams) with concrete strength of 35 MPa. The 25 MPa and 35 MPa characteristic strengths were used for their widely using and reasonable cost. The dimensions of the solid rectangular cross section of each beam were 300 mm in depth and 120 mm in width. with a 2200 mm overall longitudinal length. There were two different kinds of reinforcing bars used: high tensile steel bars that measured 10 mm in diameter and GFRP bars that had diameters of 8 and 10 mm.

2.1 Test Specimens

As seen in Figure (1), the beams were tested under two concentrated loads till failure. Two distinct reinforcement ratios, 0.5% and 1.0%, were selected for assessing the test specimens' flexural behavior. The beams were coded through the number of tension bars and the reinforcement type (S for steel and G for GFRP) followed by the rebar diameter in mm and the concrete characteristic strength in MPa. For example, 3G8-25 represents a beam reinforced with three GFRP bars of 8-mm diameter and has a concrete strength of 25 MPa. Table (1) shows the test matrix. Figure (2) and Figure (3) depict the general reinforcing details of the beams in the longitudinal section and the specimens' cross-sectional features.

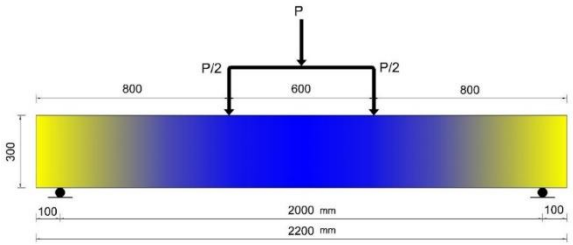

Figure 1- Loading configuration for flexural test.

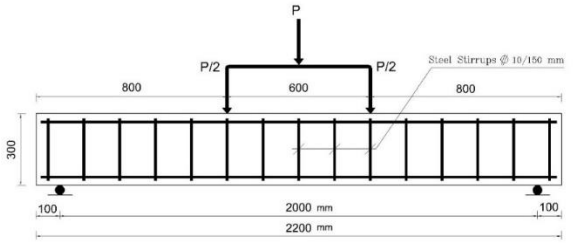

Figure 2- Reinforcement details of beams.

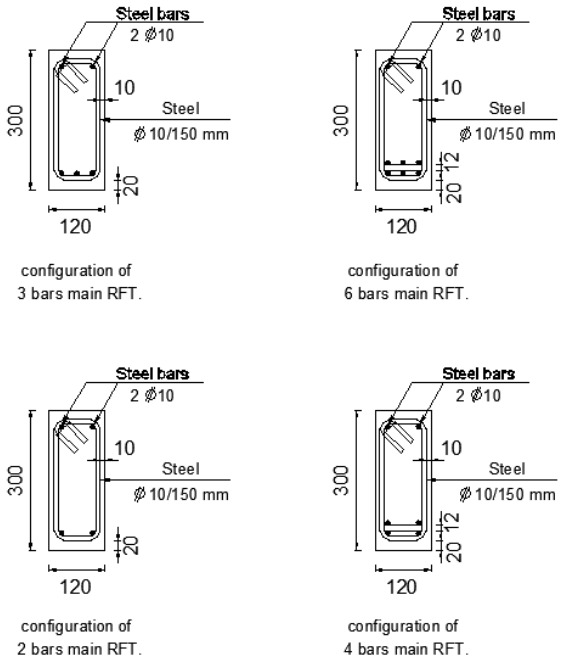

Figure 3- Cross section details of the specimens.

Table 1- Test matrix

Group	Series	Beam code	Concrete strength, f_{cu} (MPa)	Bottom reinforcement	Area of bottom reinforcement (mm^2)	Bottom reinforcement ratio, ρ (%)	Reinforcement configuration
A	I	2S10-25	25	2D10	157	0.5	1 row
		4S10-25	25	4D10	314.16	1.0	2 rows
	II	2S10-35	35	2D10	157	0.5	1 row
		4S10-35	35	4D10	314.16	1.0	2 rows
B	III	3G8-25	25	3D8	150.79	0.5	1 row
		6G8-25	25	6D8	301.59	1.0	2 rows
		2G10-25	25	2D10	157	0.5	1 row
		4G10-25	25	4D10	314.16	1.0	2 rows
	IV	3G8-35	35	3D8	150.79	0.5	1 row
		6G8-35	35	6D8	301.59	1.0	2 rows
		2G10-35	35	2D10	157	0.5	1 row
		4G10-35	35	4D10	314.16	1.0	2 rows

2.2 Materials

i. A maximum nominal size of 16 mm of crushed dolomite was utilized as the coarse material in the mix.
ii. Naturally occurring siliceous sand with sizes ranging from 0.075 to 4.75 mm was utilized as the fine aggregate in the mixture.
iii. Ordinary Portland cement was used.
iv. The mixing and curing procedures involved the use of regular tap water devoid of any flavors, fragrances, or colors.
v. For concrete mix of 35 MPa characteristic strength, Admixture of type G was used to produce high-strength concrete that contains a low cement content.
vi. There were two kinds of reinforcing bars utilized. The first was made locally of 10 mm high tensile steel. Tension test on steel bars conducted to determine the yield stress, ultimate strength, modulus of elasticity, and elongation. The test findings are listed in Table (2). The second item is GFRP bars, which are available for purchase in markets and have diameters of 8 and 10 mm. They were imported from Russia. By executing tension test on GFRP bars, the ultimate strength, modulus of elasticity, and elongation were determined. The test findings are listed in Table (3).

2.3 Concrete Mix Design

The concrete mixtures used for the specimens were prepared in compliance with Egyptian standards ECP 203-2020.

The concrete mixes were developed to achieve characteristic strengths of 25 MPa and 35 MPa after 28 days, as shown in Table (4). Following the testing of six cubes measuring 150 by 150 by 150 mm for each group, Table (5) shows the compressive strength for each group. As seen in Figure (4,5), the specimens were cast in wooden forms. After removing the beams from the forms, the specimens were cured.

Table 2- Mechanical properties of steel reinforcement.

Description	Value
Specific gravity	7.85
Yield stress (MPa)	500
Tensile strength (MPa)	630
Elongation (%)	14
Modulus of elasticity (MPa)	200000

Table 3- Mechanical properties of GFRP reinforcement.

Description	Value
Specific gravity	1.9
Tensile strength (MPa)	800
Elongation (%)	2.2
Modulus of elasticity (MPa)	40000

2.4 Strain gauge and (LVDTs)

For all specimens, one electrical strain gauge was installed on one of the main reinforcement rebars. Strain gauges used were made by Tokyo measuring instruments lab, of the type Flab-6-11-1LJC-F, with a gauge length = 6 mm, gauge resistance = 120 $\pm$ 0.5 ohms, gauge factor = 2.08 $\pm$ 1%, coefficient of thermal expansion = $11.8 \times 10\text{^}(-6)/℃$, and transvers sensitivity = 0.4 %. As illustrated in Figure

(6), the strain gauges were placed on the bars following surface cleaning and smoothing. To measure the deflection that occurred during loading, two linear variation displacement transducers (LVDTs) with a length of 100 mm were fastened to the bottom surface of the beam. One of the transducers was positioned in the middle of the beam and the other was placed under load.

Table 4- Properties of concrete mixes used.

Material	**F_{cu} = 25 MPa**	**F_{cu} = 35 MPa**
Coarse aggregates (Kg/beam)	104.7	97.4
Fine aggregates (Kg/beam)	52.4	66.1
Cement (Kg/beam)	30.45	30.45
Water (Kg/beam)	16.53	13.75
Admixtures (Kg/beam)	0	0.57

Table 5- Compressive strength for specimens after 28 days from casting.

Group	**Compressive strength in N/mm^2**
A	25
B	35

Figure 4- Wooden forms for specimens.

2.5 Testing Setup and Procedures

All beams were tested at Menoufia University's reinforced concrete laboratory. The experimental setup is shown schematically in Figure (7). All specimens were tested over a simply supported clear span of 2000 mm with bearing rods of diameter 40 mm at each support. The testing load was applied using a 200-ton hydraulic jack. The concentrated load was located at 1000 mm (mid span) from the center of the supports and turned into two-point load at 300 mm from mid span. Figure (8) shows the actual setup of the test. The data logger system is connected to a load cell, LVDTs and strain gauge at the same time connected to a computer with software program to record the data.

Figure 5- Casting the fresh concrete.

Figure 6- Setting the strain gauge on bars.

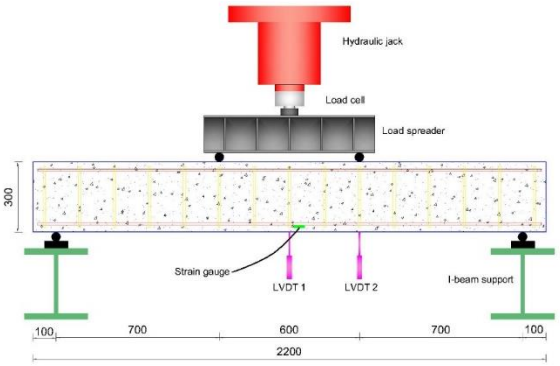

Figure 7- Schematic diagram of experimental setup.

Figure 8- Actual setup of tests.

3. Experimental Test Results

3.1 Crack Pattern

With the increasing load, the vertical flexural cracks started to form on the specimens' bottom surface and other cracks such as flexure shear cracks and web shear cracks initiated. Little branches also begin to form when these cracks move in the direction of the compression zone. However, there is a noticeable decrease in the creation of new cracks as it gets closer to the ultimate load, but there is also a noticeable widening of the existing cracks. In contrast to the GFRP RC beams, which have bigger cracking widths and wider crack spacing, the steel RC beams display closely spaced cracks. Additionally, it was noted that the cracks are bigger when the GFRP reinforcement ratio is lower. It was observed that in beams had one row of GFRP bars, all the bars were ruptured at the crossing point with stirrups under the load causing failure pattern like local shear failure in those specimens. Figure (9) and Figure (10) depict the tested beams' crack patterns.

3.2 Failure Modes

Figure (11) and Figure (12) depict the failure shape of the beams that were tested. The steel-bar-reinforced beams exhibit a ductile failure, or tension failure, in which the reinforcing bars yield before the concrete achieves its maximum strain, according to test results and the failure shape of the tested beams. When the concrete develops its maximum strain before the reinforcement bars reach their ultimate strength, the bars collapse due to concrete crushing failure (compression failure) in the 1.0% reinforcement ratio reinforced GFRP beams. The 0.5% reinforcement ratio beams reinforced with GFRP bars failed in tension due to GFRP rupture.

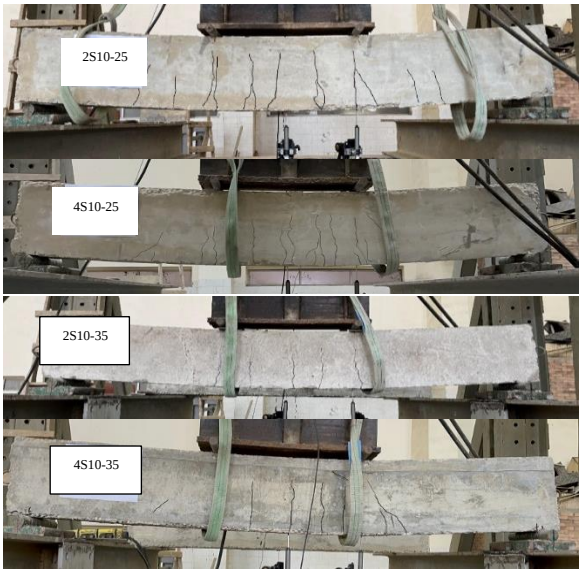

Figure 9- Crack pattern for beams of group A

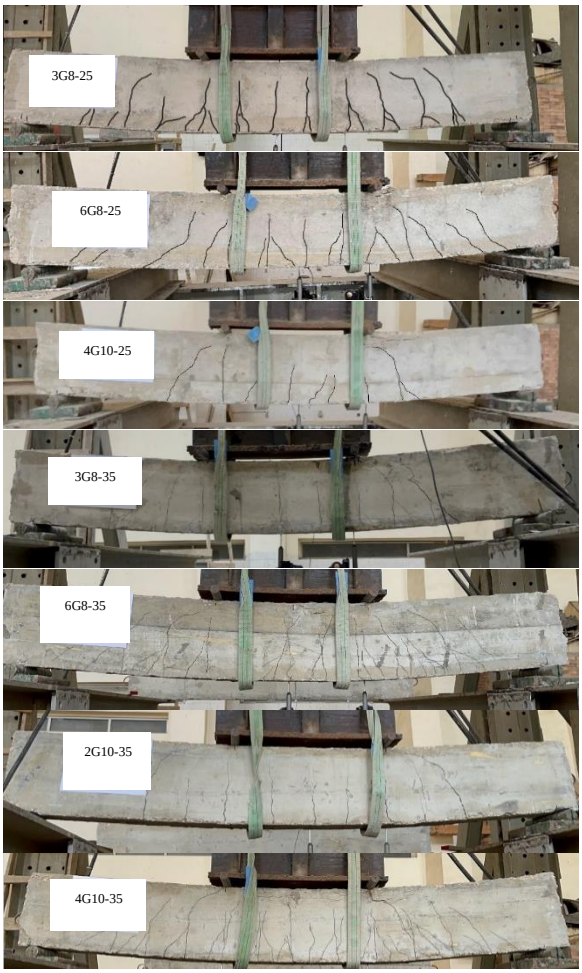

Figure 10- Crack pattern for beams of group B.

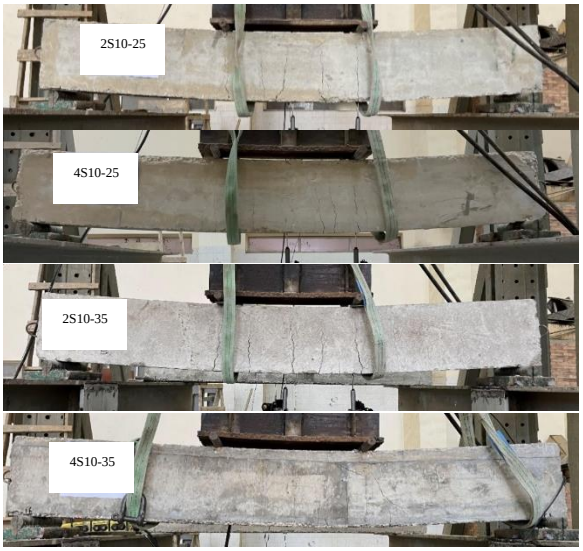

Figure 11- Failure shape for beams of group A.

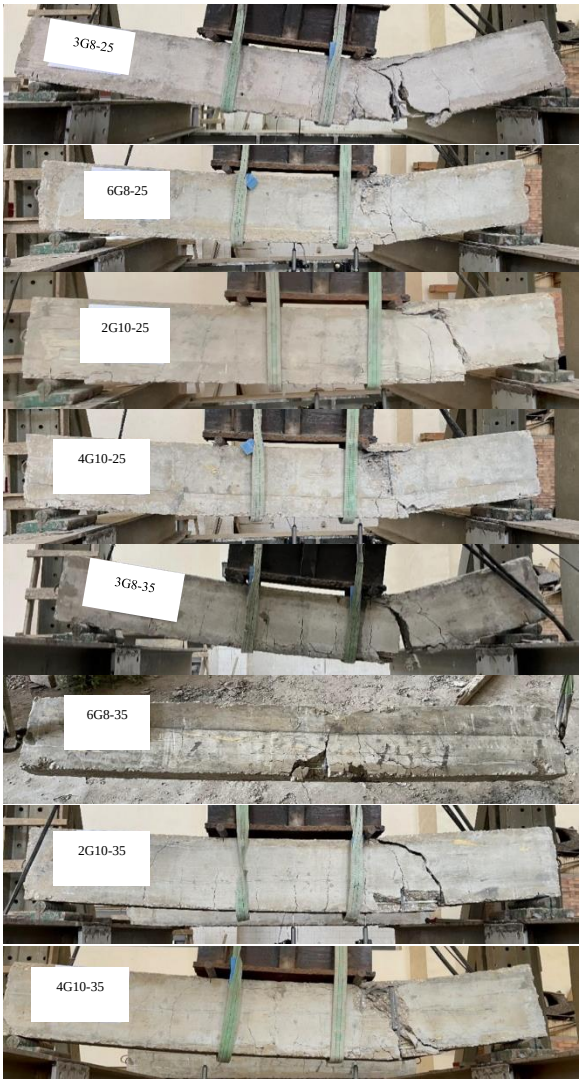

Figure 12- Failure shape for beams of group B.

3.3 Initial Cracking Loads

Figure (13) shows a comparison of the initial cracking loads for all the tested beams. It was shown that employing GFRP bars, as opposed to steel bars, reduced the initial cracking load in beams having a 0.5% reinforcement ratio with the same amount and diameter of rebars by 24% and 30% for beams of 25 MPa and 35 MPa concrete strength, respectively. And also, the initial cracking load decreased in beams having a 1.0% reinforcement ratio with the same amount and diameter of rebars by 16% and 31% for beams of 25 MPa and 35 MPa concrete strength, respectively.

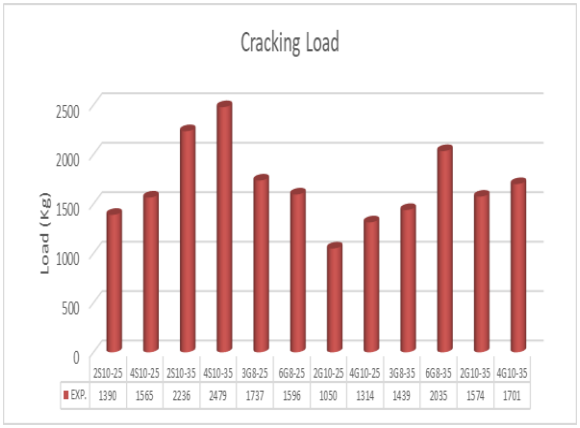

Figure 13- Comparison between initial cracking loads for different tested beams.

3.4 Failure Loads

Figure (14) shows A comparison of failure loads for all tested beams. When GFRP bars were used instead of steel bars, it became apparent that the failure load increased. Using GFRP bars in beams of 25 MPa concrete strength increased the failure load by an average of 18% and 7% while beams of 35 MPa concrete strength increased by an average of 22% and 11% for beams of 0.5% and 1.0% reinforcement ratio, respectively. When reinforcement ratio increased from 0.5% to 1.0% for the beams reinforced with GFRP bars, The failure load increased by an average of 54% and 60% for beams of 25 MPa and 35 MPa concrete strength, respectively. It was found that increasing the grade of the concrete in beams reinforced with GFRP bars increased the failure load by ratios higher than beams reinforced with steel bars. When concrete strength increased from 25 MPa to 35 MPa for beams reinforced with GFRP bars, the failure load increased by an average of 9% and 12%, while beams reinforced with steel bars increased by 5% and 8% for beams with a 0.5% and 1.0% reinforcement ratio, respectively.

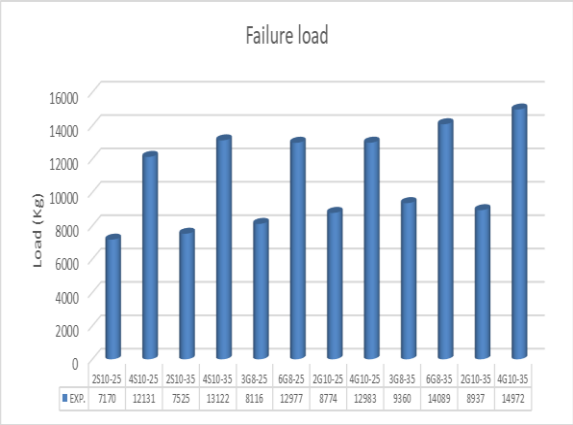

Figure 14- Comparison between failure loads for different tested beams.

3.5 Deflection Values

Figures from Figure (15) to Figure (19) show a comparison of the load-deflection curves for the specimens. When employing GFRP, it was observed that as the cracking load is reached, there is a decline in slope following the initial linear branch with a sharp slope that corresponds to the uncracked section. Up to the ultimate failure load, the post-cracking behavior of GFRP bars is almost linear. This results from the GFRP reinforcement's lack of ductility. GFRP reinforced beams show higher deflection and lower flexural rigidity as compared to steel reinforced beams. Using GFRP bars in beams of 25 MPa concrete strength increased the deflection value by an average of 21% and 90% while beams of 35 MPa concrete strength increased by an average of 26% and 51% for beams of 0.5% and 1.0% reinforcement ratio, respectively.

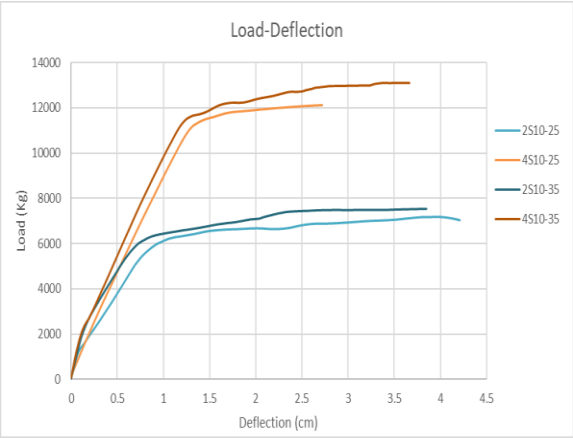

Figure 15- Load deflection curve (at mid span) for beams of group A.

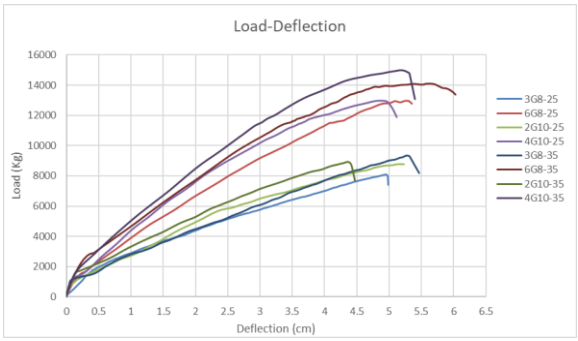

Figure 16- Load deflection curve (at mid span) for beams of group B.

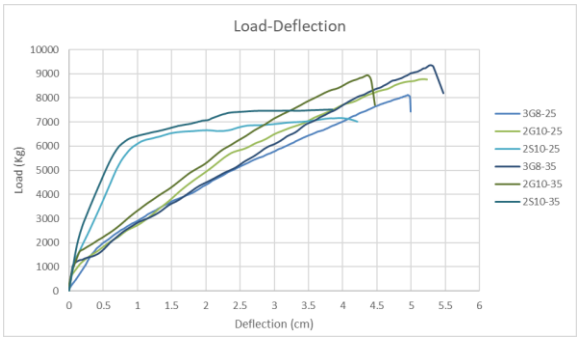

Figure 17- Load deflection curve (at mid span) for beams of 0.5% reinforcement ratio.

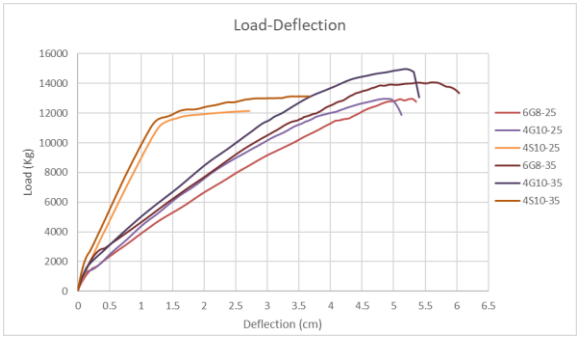

Figure 18- Load deflection curve (at mid span) for beams of 1.0% reinforcement ratio.

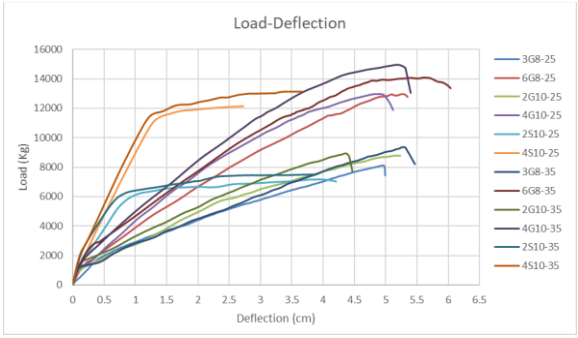

Figure 19- Load deflection curve (at mid span) for all beams.

3.6 Ductility and Energy Absorption

A structure's ductility is essential to its safety since inadequate ductility can result in a sudden, brittle failure. There are numerous definitions for ductility and ductility indices of structures, and most of them were developed with the assumption that steel is used for reinforcement. Furthermore, in most of those formulas, the yield point of the reinforcing steel is typically utilized as the reference base. FRP materials, on the other hand, exhibit a linear stress-strain relationship without plastic deformation up until the failure point. Furthermore, unlike steel beams, the energy released upon failure in fiber-reinforced polymer (FRP) beams is linear [33]. Three categories were established for these indices: conventional, displacement-based, and energy-based. Conventional ductility indices are exclusive to ductile reinforcements, but indices based on displacement and energy can be applied to both non-ductile and ductile reinforcements [34]. A recommended model was put out to calculate the ductility (μ) of fiber-reinforced polymer beams [35]. as shown in Eq. (1).

$$\mu = \frac{E_{total}}{E_{@0.75Pmax}} \quad (1)$$

The energy absorption and ductility values for all tested beams are shown in Figure (20) and Figure (21), respectively.

It is evident from the figure that the ductility index decreased from an average of 1.22 to 1.11 (by about 9%) when using GFRP bars as compared to using steel bars.

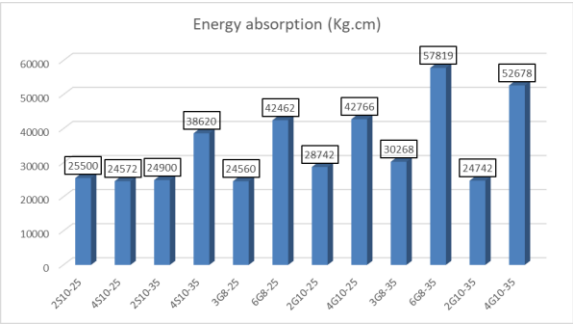

Figure 20- Energy absorption values for tested beams.

3.7 Design of Beams

Table (6) presents the analytical outcomes of the beam failure loads derived from ACI 318-19, ACI440.1R15 (Equations from Eq. (2) to Eq. (8)), ECP203-2020, and ECP 208-2005 (Equations from Eq. (9) to Eq. (15)).

$$\rho_{fb} = 0.85 \frac{f'_c}{f_{fu}} . \beta_1 . \frac{E_f . \varepsilon_{cu}}{E_f . \varepsilon_{cu} + f_{fu}} \quad (2)$$

Where β_1 is taken as 0.85 for concrete strength up to 28 MPa and reduced by 0.05 for each 7 MPa increase in f'_c but is not taken as less than 0.65.

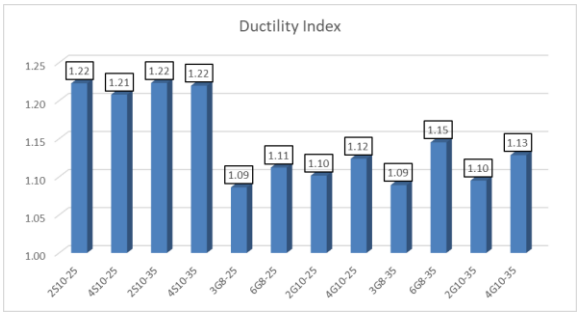

Figure 21- Ductility values for tested beams.

$$M_n = A_f . f_f . \left(d - \frac{a}{2}\right) \text{ over reinforced design} \quad (3)$$

$$a = \frac{A_f . f_f}{0.85\, f'_c\, b} \quad (4)$$

$$f_f = E_f \varepsilon_{cu} \frac{(\beta_1 d - a)}{a} \quad (5)$$

$$M_n = A_f . f_{fu} . \left(d - \frac{\beta_1 c_b}{2}\right) \text{ Under reinforced design} \quad (6)$$

$$c_b = \frac{\varepsilon_{cu}}{\varepsilon_{cu} + \varepsilon_{fu}}\, d \quad (7)$$

$$f_{fu} = C_E f^*_{fu} \quad (8)$$

Where C_E is taken as 1.0 for the comparison with the experimental flexural strength.

$$\mu_{fb} = 0.8 \frac{0.67\, f_{cu}}{f^*_{fu}} . \frac{E_f . \varepsilon_{cu}}{E_f . \varepsilon_{cu} + f^*_{fu}} \quad (9)$$

$$M_u = A_f . \frac{f^*_{fe}}{\gamma_f} . \left(d - \frac{a}{2}\right) \text{ over reinforced design} \quad (10)$$

$$a = \frac{\frac{A_f f^*_{fe}}{\gamma_f}}{\frac{0.67\, f_{cu}}{\gamma_c}\, b} \quad (11)$$

$$\frac{f^*_{fe}}{\gamma_f} = \left(\frac{0.8d - a}{a}\right) E_f . \varepsilon_{cu} \quad (12)$$

$$M_u = 0.8 \left(\frac{A_f f^*_{fu}}{\gamma_f}\right) \left(d - \frac{0.8\, c_b}{2}\right)$$

under reinforced design (13)

$$c_b = \frac{\varepsilon_{cu}}{\varepsilon_{cu} + \varepsilon^*_{fu}}\, d \quad (14)$$

$$f^*_{fu} = C_E . f_{fu} \quad (15)$$

Where C_E, γ_c and γ_f is taken as 1.0 for the comparison with the experimental flexural strength.

The impact of reinforcing in the compression zone is considered in these results. This phenomenon causes the failure of beams with a 0.5% GFRP bar reinforcement ratio to shift from compression to tension failure.

To prevent shear failure, stirrups of 10 mm diameter each 150 mm were used which give a capacity of 3.19 N/mm^2 according to ECP as shown in Eq. (16). According to experimental failure loads and by taking into consideration the own weight of beams, the maximum shear force for beams of 25 MPa was in B4 which equals 66.3 KN with an actual stress of 2.17 N/mm^2, and for beams of 35 MPa was in B10 which equals 76.3 KN with an actual stress of 2.5 N/mm^2.

Table 6– Failure loads of the beams by using equations of ACI 440.1R-15, ACI 318-19, ECP 208-2005 and ECP 203-2020.

Group	Series	Beam Code	Failure load (Kg)		Type of section
			ACI	ECP	
A	I	2S10-25	5514	5509	Under reinforced
		4S10-25	10057	10057	Under reinforced
	II	2S10-35	5869	5629	Under reinforced
		4S10-35	10289	10083	Under reinforced
B	III	3G8-25	8660	6952	Under reinforced
		6G8-25	10469	10199	Over reinforced
		2G10-25	8983	7211	Under reinforced
		4G10-25	10466	10195	Over reinforced
	IV	3G8-35	8660	6952	Under reinforced
		6G8-35	11974	11640	Over reinforced
		2G10-35	8983	7211	Under reinforced
		4G10-35	11983	11648	Over reinforced

$$q_{st} = \frac{n\, A_s\, f_y/\gamma_s}{b\, .s} \quad (16)$$

Where f_y equals 420 MPa and γ_s equals 1.15 according to ECP203-2020.

A comparison of experimental and analytical failure loads for several tested beams is shown in Figure (22). Good results from the analysis match the outcomes of the experimental tests.

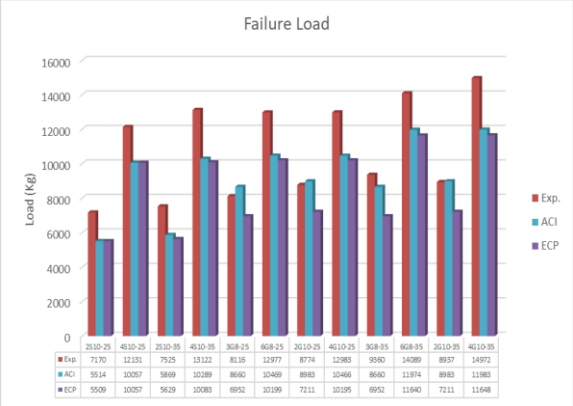

Figure 22- Comparison between experimental and analytical failure loads for different tested beams.

4. Finite Element Model

A common numerical method used in structures and structural components is finite-element analysis (FEA) [36]–[38]. All the samples were numerically simulated using the FE program "ABAQUS Release 6.14" to study their flexural behavior up to failure.

4.1 Material Properties

The compressive and tensile stress-strain curves for the concrete were integrated into ABAQUS to account for the nonlinearity of the material. The Concrete Damaged Plasticity (CDP) model in ABAQUS was used to simulate concrete damage [39]–[41]. For the steel used in the beams, an elastic modulus of 200 GPa and a Poisson's ratio of 0.3 were determined. A yield stress of 500 MPa was determined. The GFRP bars exhibit a linear stress-strain curve up until rupture, in contrast to the ductility of steel. To simulate this behavior, just the modulus of elasticity (40 GPa) and Poisson's ratio (0.25) were added to the GFRP material model.

Linear hexahedral reduced integration 3-D stress elements (C3D8R), which have eight nodes and three degrees of freedom (DOF) each, are used to simulate the concrete beam. GFRP and steel bars are modelled with T3D2, which are 2-node linear 3-D truss elements with three degrees of freedom per node [42], [43]. Rigid constraints apply to the load and support bearing plates. The connectivity between the bars and the beam is defined through the application of an embedded-type constraint, where the steel reinforcement acts as the embedded region and the concrete beam acts as the host region. Figure (23) displays the reinforcement cage for a beam in addition to the concrete beam model.

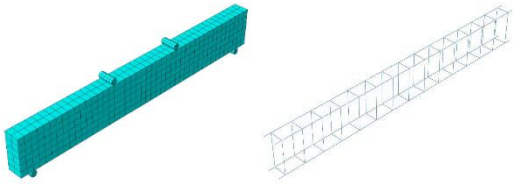

Figure 23- The reinforcement cage for a beam in addition to the concrete beam model.

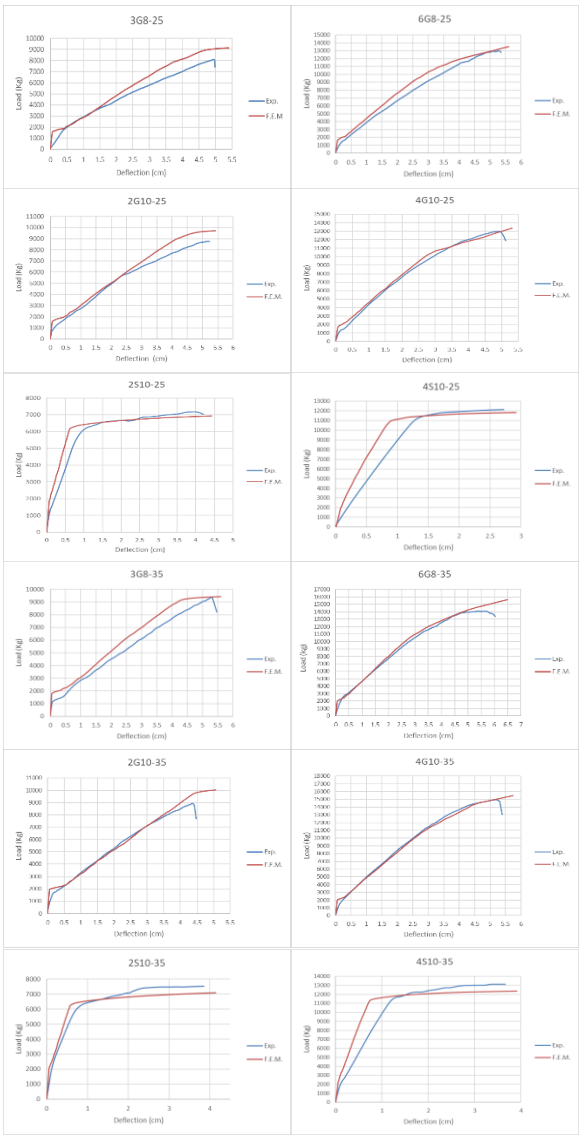

Figure 24- The comparison of the load-deflection relationship between the FE model prediction and the experimental data.

4.2 Modelling

The accuracy of the FE models was confirmed by comparing the load versus deflection responses obtained for the same beam with the outcomes of experiments. Figure (24) gives the comparison of the load-deflection relationship between the FE model prediction and the experimental data for all tested beams. It is evident from the subplots in the figures that the finite element model that was created can accurately predict the behavior of beams with respect to their initial stiffness, ultimate failure load, and load-corresponding deflection during the loading process until failure. The results show good agreement in every case, with a few minor variations in the initial stiffness. This divergence from the experimental findings could be due to the anticipated variation in the tensile characteristics of the concrete material.

5. Finite Element Results

Figures from Figure (25) to Figure (29) illustrate comparison between load-deflection curves for FE models. The results show good agreement in every case, with a few minor variations in the initial stiffness. This divergence from the results of the experiments could be explained by an expected variation in the concrete material's tensile characteristics. Table (7) provides a summary of the first crack and ultimate loads determined by experimental, analytical, and numerical study. Figure (30) shows the differences between experimental, analytical, and numerical results for failure loads. Numerical analysis results are in good agreement with analytical and experimental results.

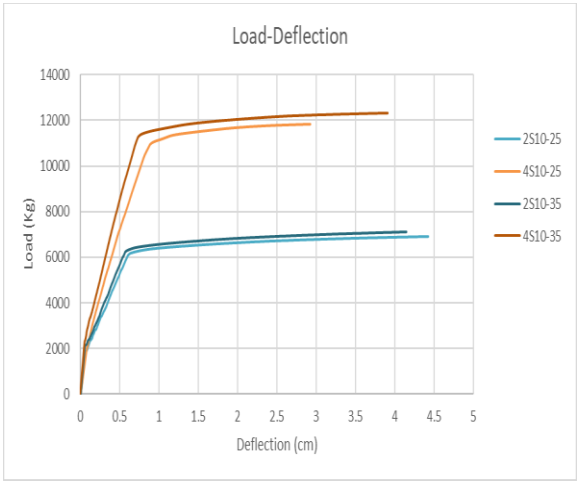

Figure 25- Load deflection curves from FE models for group A.

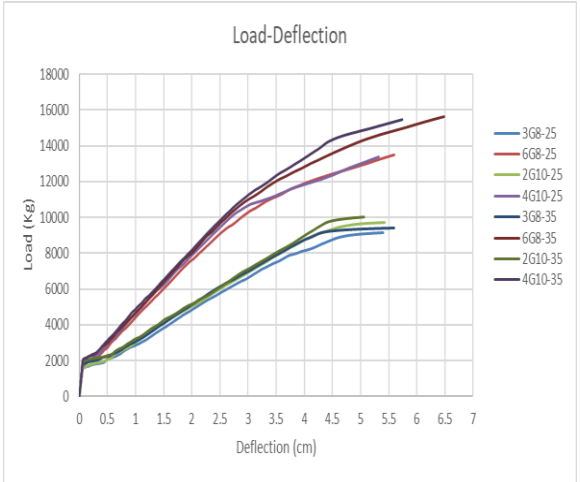

Figure 26- Load deflection curves from FE models for group B.

Table 7- First crack and failure loads determined by experimental, analytical, and numerical study.

Beam code	First crack load (Kg)				Failure load (Kg)			
	Exp.	ACI	ECP	FEM	Exp.	ACI	ECP	FEM
2S10-25	1390	1505	1620	1821	7170	5514	5509	6923
4S10-25	1565	1505	1620	1965	12131	10057	10057	11853
2S10-35	2236	1780	1917	2075	7525	5869	5629	7102
4S10-35	2209	1780	1917	2252	13122	10289	10083	12342
3G8-25	1737	1505	1620	1476	8116	8660	6952	9152
6G8-25	1596	1505	1620	1613	12977	10469	10199	13507
2G10-25	1050	1505	1620	1475	8774	8983	7211	9718
4G10-25	1314	1505	1620	1729	12983	10466	10195	13391
3G8-35	1439	1780	1917	1772	9360	8660	6952	9412
6G8-35	2035	1780	1917	2018	14089	11974	11640	15639
2G10-35	1574	1780	1917	1938	8937	8983	7211	10027
4G10-35	1701	1780	1917	2112	14972	11983	11648	15473

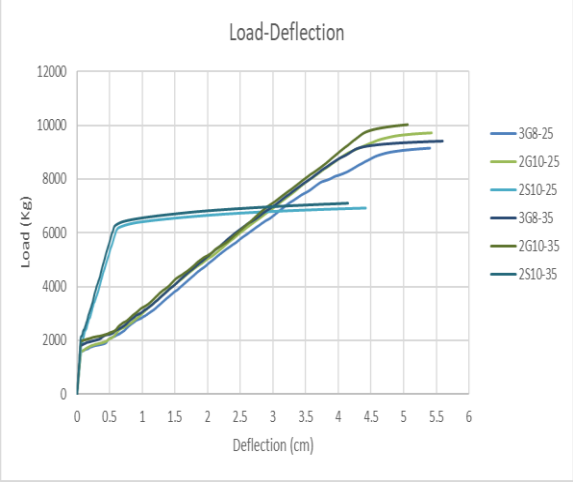

Figure 27- Load deflection curves from FE models for beams of 0.5% reinforcement ratio.

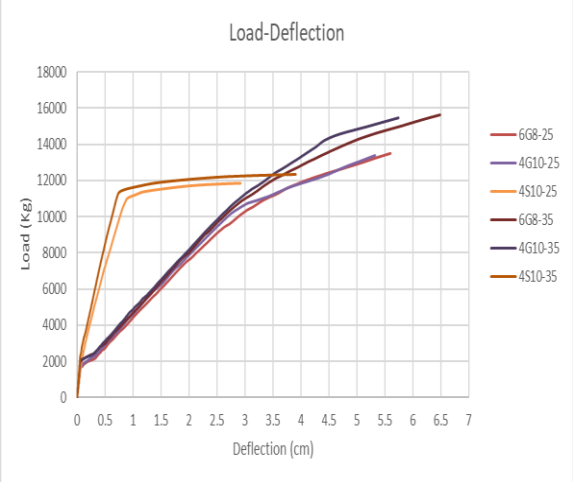

Figure 28- Load deflection curves from FE models for beams of 1.0% reinforcement ratio.

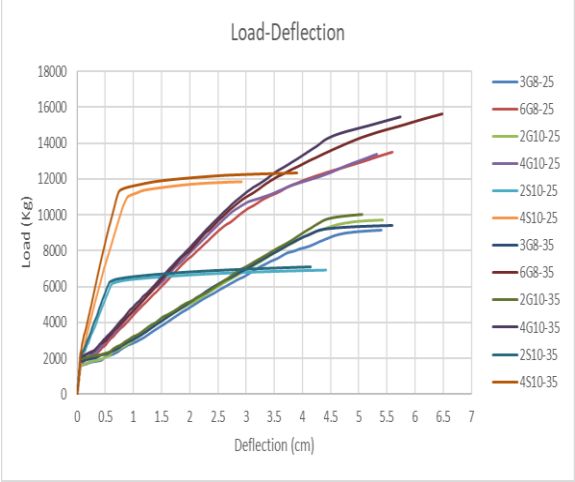

Figure 29- Load deflection curves from FE models for all models.

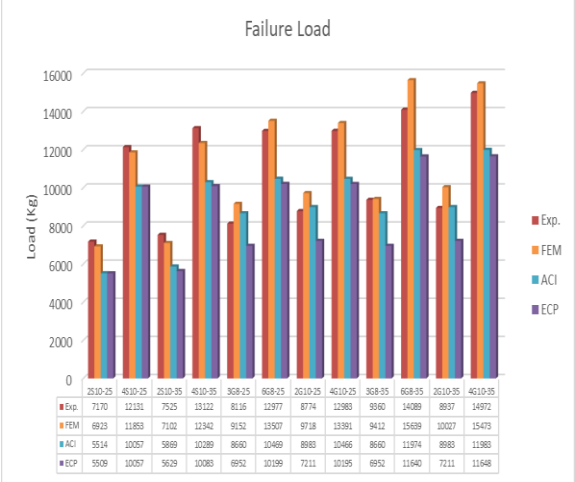

Figure 30- Failure loads comparison between experimental, analytical, and numerical studies.

5. Conclusions

From the present study, the following conclusions are obtained:

1- For the same amount and diameter of reinforcement, using GFRP bars instead of steel bars reduced the initial cracking load in beams having a 0.5% reinforcement ratio by 24% and 30% for beams of 25 MPa and 35 MPa concrete strength, respectively.
2- For the same amount and diameter of reinforcement, using GFRP bars instead of steel bars decreased the initial cracking load in beams having a 1.0% reinforcement ratio by 16% and 31% for beams of 25 MPa and 35 MPa concrete strength, respectively.
3- For the same reinforcement ratio and the same grade of concrete, using GFRP bars of diameter 10 mm led to approximately equal or slightly increased initial cracking load compared to GFRP bars of diameter 8 mm.
4- Using GFRP bars in beams of 25 MPa concrete strength increased the failure load compared to steel bars by an average of 18% and 7% for beams of 0.5% and 1.0% reinforcement ratio, respectively.
5- Using GFRP bars in beams of 35 MPa concrete strength increased the failure load compared to steel bars by an average of 22% and 11% for beams of 0.5% and 1.0% reinforcement ratio, respectively.
6- When reinforcement ratio increased from 0.5% to 1.0% for the beams reinforced with GFRP bars, The failure load increased by an average of 54% and 60% for beams of 25 MPa and 35 MPa concrete strength, respectively.
7- For the same reinforcement ratio and the same grade of concrete, using GFRP bars of diameter 10 mm led to approximately equal or slightly increased the failure load compared to GFRP bars of diameter 8 mm.
8- Increasing the grade of the concrete in beams reinforced with GFRP bars increased the failure load by ratios higher than beams reinforced with steel bars.
9- When concrete strength increased from 25 MPa to 35 MPa for beams reinforced with GFRP bars, the failure load increased by an average of 9% and 12%, while beams reinforced with steel bars increased by 5% and 8% for beams with a 0.5% and 1.0% reinforcement ratio, respectively.
10- GFRP reinforced beams show higher deflection and lower flexural rigidity as compared to steel reinforced beams.
11- Using GFRP bars in beams of 25 MPa concrete strength increased the deflection value by an average of 21% and 90% while beams of 35 MPa concrete strength increased by an average of 26% and 51% for beams of 0.5% and 1.0% reinforcement ratio, respectively.
12- For the same reinforcement ratio and the same grade of concrete, using GFRP bars of diameter 10 mm led to approximately equal or slightly decreased the deflection value compared to GFRP bars of diameter 8 mm.
13- For steel-reinforced beams, ACI 318-19 and ECP 203-2020 give almost the same failure loads and underestimate the failure loads compared to experimentally obtained results.
14- For under-reinforced sections in beams reinforced with GFRP bars, ECP 208-2005 underestimates the failure loads compared to ACI 440.1R-15 which gives good results with experimentally obtained results.
15- For over-reinforced sections in beams reinforced with GFRP bars, ACI 440.1R-15 and ECP 208-2005 give almost the same failure loads and underestimate the failure loads compared to experimentally obtained results.
16- The ductility index decreased from an average of 1.22 to 1.11 (by about 9%) when using GFRP bars as compared to using steel bars.

6. Notation

A_f	area of FRP tension reinforcement, mm^2
A_s	area of steel bar, mm^2
a	the depth of equivalent rectangular stress block, mm
b	effective width of beam, mm
c	distance from extreme compression fiber to the neutral axis, mm
c_b	distance from extreme compression fiber to the neutral axis at balanced condition, mm
C_E	environmental reduction factor
d	distance from extreme compression fiber to centroid of tension force, mm
E_c	modulus of elasticity of concrete, MPa
E_S	modulus of elasticity of steel reinforcement, MPa
E_f	modulus of elasticity of FRP reinforcement, MPa
f_c'	cylinder compressive strength of concrete, MPa
f_{cu}	cube compressive strength of concrete, MPa
f_f	stress in FRP reinforcement under specified loads according to ACI, MPa
f_{fu}	designed tensile strength of GFRP bars according to ACI, MPa

f_{fu}	tensile strength of GFRP bars according to ECP, MPa
f^*_{fu}	tensile strength of GFRP bars according to ACI, MPa
f^*_{fu}	designed tensile strength of GFRP bars according to ECP, MPa
f^*_{fe}	stress in FRP reinforcement under specified loads according to ECP, MPa
f_y	yield strength of steel longitudinal reinforcement, MPa
M_n	nominal moment of reinforced concrete section according to ACI, KN.m
M_u	ultimate limit moment according to ECP, KN.m
n	number of branches for stirrups.
q_{st}	shear resistance provided by steel stirrups, MPa
s	stirrup spacing, mm
ε_{cu}	ultimate strain of concrete
ε_{fu}	ultimate strain in GFRP
ρ_f	longitudinal reinforcement ratio
ρ_{fb}, μ_{fb}	balanced longitudinal reinforcement ratio
β_1	factor of the equivalent stress block depth
γ_c , γ_f	strength reduction factor for concrete and FRP bars
γ_s	strength reduction factor steel bars

7. References

[1] O. Gouda, A. Asadian, and K. Galal, "Flexural and Serviceability Behavior of Concrete Beams Reinforced with Ribbed GFRP Bars," J. Compos. Constr., vol. 26, no. 5, 2022, doi: 10.1061/(asce)cc.1943-5614.0001253.

[2] M. M. Kamal, M. A. Safan, and R. A. Salama, "Experiments on strengthened concrete beams with hybrid steel-grfp rebars," ERJ. Eng. Res. J., vol. 31, no. 2, pp. 201–210, Apr. 2008, doi: 10.21608/erjm.2008.69535.

[3] Chidananda S. H and R. B. Khadiranaikar, "Flexural behaviour of concrete beams reinforced with GFRP Rebars," Int. J. Adv. Res. Ideas Innov. Technol., vol. 3, no. 5, pp. 119–128, 2017.

[4] M. M. Safaan, "Mechanical properties of locally produced hybrid frp bars as concrete reinforcement," Proc. Int. Conf. Futur. Vis. Challenges Urban Dev. Hous. Build. Res. Cent. (HBRC), Cairo, Egypt, 20-22 December 2004. HBRC Journal, Vol. 1, No. 1, December 2004, ISSN 12479/2004, 1-13.

[5] M. Kamal, M. Safaan, and M. Al-Gazzar, "Ductility of concrete beams reinforced with hybrid FRP rebars," HBRC J, Hous \& Build Res Cent, vol. 2, no. 3, pp. 1–12, 2006.

[6] M. Elsedemy, M. Kandil, and N. N. Meleka, "A State-of-the-Art Review on the behavior of RC beams with different types of FRP Reinforcement," Eng. Res. J., vol. 45, no. 4, pp. 591–600, 2022.

[7] M. A. Muhammad and F. R. Ahmed, "Evaluation of deflection and flexural performance of reinforced concrete beams with glass fiber reinforced polymer bars," *Case Stud. Constr. Mater.*, vol. 18, no. January, p. e01855, 2023, doi: 10.1016/j.cscm.2023.e01855.

[8] O. I. Abdelkarim, E. A. Ahmed, H. M. Mohamed, and B. Benmokrane, "Flexural strength and serviceability evaluation of concrete beams reinforced with deformed GFRP bars," *Eng. Struct.*, vol. 186, no. May 2018, pp. 282–296, 2019, doi: 10.1016/j.engstruct.2019.02.024.

[9] B. Chhorn, S. Lee, and W. Jung, "Comparison Study on Flexural Behavior of Steel and FRPs Reinforced Concrete Beam," *Int. J. Steel Struct.*, vol. 23, no. 3, pp. 860–871, 2023, doi: 10.1007/s13296-023-00737-z.

[10] Z. Mahaini, F. Abed, Y. Alhoubi, and Z. Elnassar, "Experimental and numerical study of the flexural response of Ultra High Performance Concrete (UHPC) beams reinforced with GFRP," *Compos. Struct.*, vol. 315, p. 117017, Jul. 2023, doi: 10.1016/j.compstruct.2023.117017.

[11] M. S. Ifrahim, A. J. Sangi, and S. H. Ahmad, "Experimental and numerical investigation of flexural behaviour of concrete beams reinforced with GFRP bars," *Structures*, vol. 56, p. 104951, 2023, doi: https://doi.org/10.1016/j.istruc.2023.104951.

[12] T. M. S. Alrudaini, "Optimization of concrete beams reinforced with GFRP bars," *J. Soft Comput. Civ. Eng.*, vol. 6, no. 3, pp. 18–38, 2022, doi: 10.22115/scce.2022.323501.1392.

[13] S. Sirimontree, S. Keawsawasvong, and C. Thongchom, "Flexural Behavior of Concrete Beam Reinforced with GFRP Bars Compared to Concrete Beam Reinforced with Conventional Steel Reinforcements," vol. 24, no. 6, pp. 883–890, 2021.

[14] X. Ruan, C. Lu, K. Xu, G. Xuan, and M. Ni, "Flexural behavior and serviceability of concrete beams hybrid-reinforced with GFRP bars and steel bars," *Compos. Struct.*, vol. 235, 2020, doi: 10.1016/j.compstruct.2019.111772.

[15] N. Kabashi, B. Avdyli, E. Krasniqi, and A. Këpuska, "Comparative approach to flexural behavior of reinforced beams with GFRP, CFRP, and steel bars," *Civ. Eng. J.*, vol. 6, no. 1, pp. 50–59, 2020, doi: 10.28991/cej-2020-03091452.

[16] S. Kim and S. Kim, "Flexural behavior of concrete beams with steel bar and FRP reinforcement," *J. Asian Archit. Build. Eng.*, vol. 18, no. 2, pp. 94–102, 2019, doi: 10.1080/13467581.2019.1596814.

[17] A. El-Nemr, E. A. Ahmed, A. El-Safty, and B. Benmokrane, "Evaluation of the flexural strength and serviceability of concrete beams reinforced with different types of GFRP bars," *Eng. Struct.*, vol. 173, no. December 2017, pp. 606–619, 2018, doi: 10.1016/j.engstruct.2018.06.089.

[18] G. Naveen Kumar and K. Sundaravadivelu, "Experimental Study on Flexural Behaviour of Beams Reinforced with GFRP Rebars," *IOP Conf. Ser. Earth Environ. Sci.*, vol. 80, no. 1, 2017, doi: 10.1088/1755-1315/80/1/012027.

[19] A. Confrere, L. Michel, E. Ferrier, and G. Chanvillard, "Experimental behaviour and deflection of low-strength concrete beams reinforced with FRP bars," *Struct. Concr.*, 2016.

[20] A. Masmoudi, M. Ben Ouezdou, and M. H. Mechanics, "MODE OF FAILURE FOR REINFORCED CONCRETE BEAMS WITH GFRP BARS," Journal of theoretical and applied mechanics, vol. 54, no. 4, pp. 1137-1146, Warsaw 2016, doi: 10.15632/jtam-pl.54.4.1137.

[21] A. S. Shanour, M. Adam, A. Mahmoud, and M. Said, "Experimental Investigation of Concrete Beams Reinforced With Gfrp Bars," International Journal of Civil Engineering and Technology (IJCIET), vol. 5, no. 11, 2015, pp. 154–164.

[22] A. El-Nemr, A. A. Ehab, and B. Benmokrane, "Flexural Behavior and Serviceability of Normal- and High-Strength Concrete Beams Reinforced with Glass Fiber-Reinforced Polymer Bars," *ACI Struct. J.*, vol. 120, no. 3, pp. 47–60, 2013, doi: 10.14359/51738502.

[23] I. F. Kara, A. F. Ashour, and C. Dundar, "Deflection of concrete structures reinforced with FRP bars," *Compos. Part B Eng.*, vol. 44, no. 1, pp. 375–384, 2013, doi: 10.1016/j.compositesb.2012.04.061.

[24] C. Miàs, L. Torres, A. Turon, and C. Barris, "Experimental study of immediate and time-dependent deflections of GFRP reinforced concrete beams," *Compos. Struct.*, vol. 96, pp. 279–285, 2013, doi: 10.1016/j.compstruct.2012.08.052.

[25] H. Qu, L. Chen, and S. Zhang, "Flexural analysis of simply supported concrete beam reinforced with FRP bars," *Appl. Mech. Mater.*, vol. 182–183, pp. 1617–1621, 2012, doi: 10.4028/www.scientific.net/AMM.182-183.1617.

[26] M. S. Issa and S. M. Elzeiny, "Flexural behavior of cantilever concrete beams reinforced with glass fiber reinforced polymers (GFRP) bars," *J. Civ. Eng. Constr. Technol.*, vol. 2, no. February, pp. 33–44, 2011.

[27] V. G. Kalpana and K. Subramanian, "Behavior of concrete beams reinforced with GFRP BARS," *J. Reinf. Plast. Compos.*, vol. 30, no. 23, pp. 1915–1922, 2011, doi: 10.1177/0731684411431119.

[28] C. Barris, L. Torres, A. Turon, M. Baena, and A. Catalan, "An experimental study of the flexural behaviour of GFRP RC beams and comparison with prediction models," *Compos. Struct.*, vol. 91, no. 3, pp. 286–295, 2009, doi: 10.1016/j.compstruct.2009.05.005.

[29] P. V Vijay and H. V. S. GangaRao, "Bending behavior and deformability of glass fiber-reinforced polymer reinforced concrete members," *Struct. J.*, vol. 98, no. 6, pp. 834–842, 2001.

[30] M. A. Safan, "Behavior and Design Aspects of Concrete Beams Reinforced With Hybrid Steel-Gfrp Bars," *ERJ. Eng. Res. J.*, vol. 35, no. 2, pp. 139–147, 2012, doi: 10.21608/erjm.2012.67128.

[31] M. A. Safaan and M. R. Afify, "Behavior of concrete beams reinforced with in-house manufactured gfrp bars," *Proc. Fourth Middle East Symp. Struct. Compos. Infrastruct. Appl. MESC-4, Alexandria, Egypt, May 20-23, 2005.*

[32] M. M. Kamal, M. A. Safan, and A. A. Bashandy, "Experiments on Using Fiber Reinforced Polymer Rebars in One-Way Concrete Slabs," *Proc. 6th Egypt. Rural Dev. Conf. Fac. Eng. Menoufia Univ. Egypt*, no. October, pp. 897–908, 2007.

[33] S. H. Alsayed and A. M. Alhozaimy, "Ductility of concrete beams reinforced with FRP bars and steel fibers," *J. Compos. Mater.*, vol. 33, no. 19, pp. 1792–1806, 1999.

[34] J. H. Ling, Y. T. Lim, and E. Jusli, "Methods to Determine Ductility of Structural Members: A Review," *J. Civ. Eng. Forum*, vol. 9, no. May, pp. 181–194, 2023, doi: 10.22146/jcef.6631.

[35] G. Spadea, F. Bencardino, R. N. Swamy, and others, "Strengthening and upgrading structures with bonded CFRP sheets: Design aspects for structural integrity," in *Proceedings of the Third International Symposium on Non-Metallic (FRP) Reinforcement for Concrete Structures*, 1997, vol. 1, pp. 629–636.

[36] H. G. Kwak and F. C. Filippou, "Finite element analysis of reinforcement concrete structures under monotonic loads," 1990.

[37] M. El-Zoughiby, "An introduction to the finite element method," 2014.

[38] D. L. Logan, "A first course in the finite element method, 5th," *Kanada Cengage Learn.*, 2011.
[39] T. Jankowiak and T. Lodygowski, "Identification of parameters of concrete damage plasticity constitutive model," *Publ. House Pozn. Univ. Technol.*, no. 6, 2005.
[40] T. Cuong-le, H. Minh, and T. Sang-to, "A nonlinear concrete damaged plasticity model for simulation reinforced concrete structures using ABAQUS," vol. 59, pp. 232–242, 2022, doi: 10.3221/IGF-ESIS.59.17.
[41] Simulia, "ABAQUS Analysis User's Manual," V 2014.
[42] R. S. Mohammed and Z. Fangyuan, "Numerical Investigation of the Behavior of Reinforced Concrete Beam Reinforced with FRP Bars," *Civ. Eng. J.*, vol. 5, no. 11, pp. 2296–2308, 2019, doi: 10.28991/cej-2019-03091412.
[43] D. Sihua, Q. Ze, and W. Li, "Nonlinear analysis of reinforced concrete beam bending failure experimentation based on ABAQUS," in International Conference on Information Sciences, Machinery, Materials and Energy (ICISMME 2015), 2015, pp. 440–444.

8. Codes and Standards

- ACI440.1R-15 (2015) Guide for the Design and Construction of Structural Concrete Reinforced with Fiber-Reinforced Polymer (FRP) Bars, American Concrete Institute.
- ACI Committee 440, Building Code Requirements for Structural Concrete Reinforced with Glass Fiber- Reinforced Polymer (GFRP) Bars—Code and Commentary (ACI 440.11-22). American Concrete Institute, Farmington Hills, MI, 2022.
- ECP 208-2005 'Using of fiber reinforced polymers Egyptian Code', Egyptian Housing and Building National Research Center.
- ECP 203-2020, "Egyptian code for design and construction of reinforced concrete structures," Ministry of Development, New Communities, Housing and Utilities, Housing and Building Research Center. 2020.
- ASTM C 33-18 (2018) 'Designation: C33/C33M−18 Standard Specification for Concrete Aggregates', ASTM InternationalC33/C33M.